



CMD 22-M37.5

Date: 2022-10-17

File / dossier : 6.02.04

Edocs pdf : 6892445

Oral presentation

Exposé oral

**Written submission from
Paul Sedran**

**Mémoire de
Paul Sedran**

**CNSC staff update on elevated
hydrogen equivalent concentration
discovery events in the pressure
tubes of reactors in extended
operation**

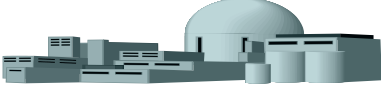
**Mise à jour du personnel de la
CCSN sur les événements liés aux
découvertes de concentrations
élevées d'hydrogène équivalent dans
les tubes de forces de réacteurs en
exploitation prolongée**

Commission Meeting

Réunion de la Commission

November 3, 2022

Le 3 novembre 2022

 RESD Inc.	Document Identification				
	<small>Project</small>	<small>Type</small>	<small>Division</small>	<small>Serial</small>	<small>Revision</small>
	CNSC 003	REPT	ENG	0001	00
<small>Date Effective:</small>			<small>Retain Until:</small>		
Oct 15, 2022			Oct 15, 2029		

Review of Bruce Power Submissions on Elevated
 Heq in Pressure Tube Rolled Joints and
 Independent Analysis of Possible Causes



Prepared by: Paul Sedran, P.Eng
 Principal, RESD Inc

Date: October 15, 2022

Record of Revisions

Rev.	Date	Description	Prepared by	Reviewed by
Draft 1	May 17 th , 2009	Draft issued to the CNSC	Paul Sedran	

1. Introduction

Based on Pressure Tube (PT) fracture toughness considerations, the Power Reactor Operating Licence (PROL 18.01/2028) for the Bruce reactors specifies a maximum allowable hydrogen equivalent (Heq) concentration of 120 ppm for the PTs.

In July, 2021, Bruce Power discovered, for the first time, that the Heq concentration in a PT in the Bruce Nuclear Generating Stations had exceeded the 120 ppm limit. In particular, the PT removed from Fuel Channel B6S13 was found to have an Heq measurement of 211 ppm at the burnish mark (BM) and 212 ppm 10 mm inboard the BM. In addition, several PTs in Bruce Unit 3 were found to exceed 120 ppm near the location of the BM.

The discovery of elevated Heq concentrations in Bruce Units 3 and 6 was communicated to the CNSC, who issued Designated Officer Orders to Bruce Power, Ontario Power Generation, and NB Power, on July 26, 2021.

As a result of the Designated Officer Orders, various documents were submitted to the CNSC by Bruce Power.

Under the auspices of the CNSC's Participant Funding Program, the Bruce Power submissions to the CNSC were reviewed independently, with the primary objective of investigating the validity of the theory that the elevated Heq concentrations observed at the top of PT B6S13 are attributable to thermal H/D diffusion from the bottom of the PT to an area of reduced temperature at the top of the PT.

The following Bruce Power documents were reviewed:

1. CNSC CMD21-H11, Signed September 3, 2021, e-Doc 6634528 (PDF).
2. Bruce Power Submission CMD 21-H11.2, September 1st, 2021, Edocs: 6630917.
3. Bruce Power Submission CMD 21-H11.2A, September 2nd, 2021, Edocs: 6633418.
4. Bruce Power Submission CMD 21-H11.2B, September 9th, 2021, Edocs: 6636949.

As part of the review, the theory that circumferential thermal diffusion of H/D from the bottom to the top of the PT was the cause of the elevated Heq measurement in B6S13 was investigated using simple closed form solutions for the circumferential diffusion of H/D in a concentration gradient, combined with a thermal gradient. In the simplified diffusion analysis, presented here, the thermal gradient required to produce the circumferential Heq concentration gradient seen in B6S13 was predicted and compared with expected thermal gradients that B6S13 would have been exposed to in service.

It should be noted that although this assessment contains some analytical work, the scope of the analysis is very limited in comparison to the volume of work produced by Bruce Power in 2021-2022. In addition, some public domain information was used instead of the complete set of up-to-date proprietary data available to Bruce Power Staff. And, in addition, formal QA verification of the calculations could not be performed within the scope of the work. As a result, the review is limited and not comprehensive enough to support definitive conclusions, without more work.

Much of the value in this assessment derives from the fact that it is not an internal quality assurance verification of the numerical work produced by Bruce Power, consisting of checking

calculations line by line. Instead, the assessment has independently used different methodologies than Bruce Power, based on the contention that an agreement of the Bruce Power analyses with an independent assessment would provide greater certainty than an in-house quality assurance verification.

2. Technical Background

2.1 Diffusion Mechanisms for H/D in the PT RJ

The rupture of PT P2G16 in August 1983 provided a drastic example of the propensity for zirconium to absorb hydrogen (H) and deuterium (D) and for H/D to diffuse within the PT, in this case with severe consequences for PT integrity. Since then, the industry has conducted research and extensive material surveillance programs that have resulted in the development of predictive models for the ingress and redistribution of H/D in PTs, one for the distribution of H/D in the body of the PT, and a separate model for the distribution in the PT Rolled Joint (RJ).

The general equation for the diffusion of H/D in the RJ of the PT is given below.

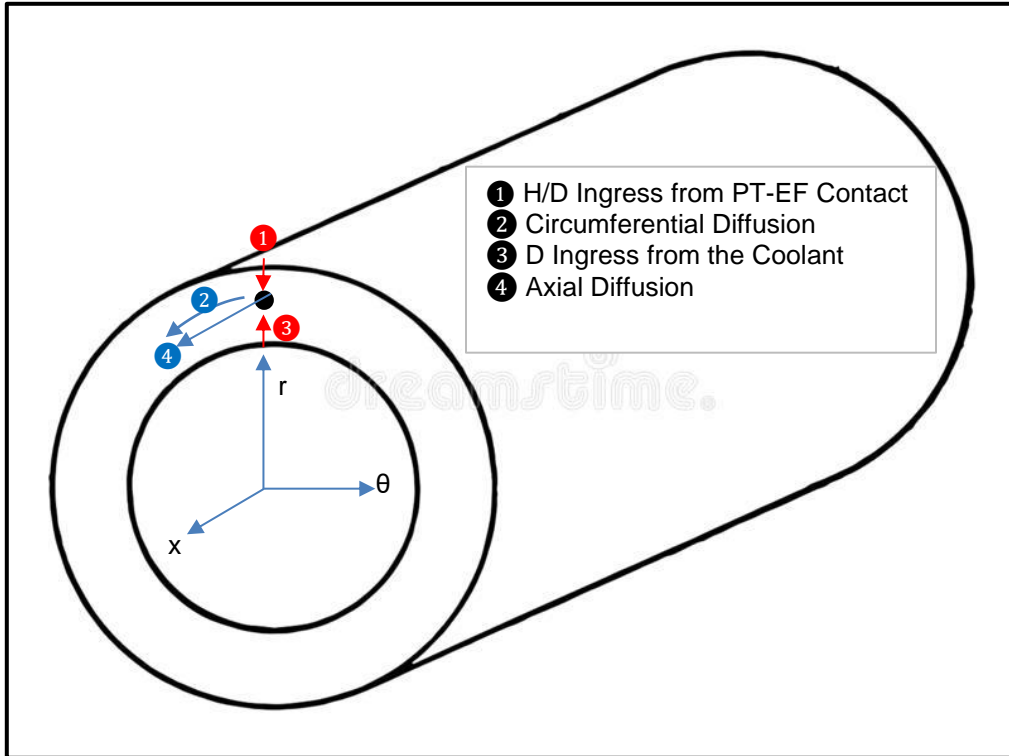
$$\text{grad}(C(x,y,z,t)) = D \nabla^2 C(x,y,z,t) + S(x,y,z,t)$$

The diffusion of H/D into the PT RJ and redistribution of H/D is determined by 2 ingress mechanisms (1 and 2, below) and three diffusion mechanisms (3, 4, and 5) :

1. Electrochemical Diffusion of H/D from the EF into the PT RJ based on Raoult's law,
2. Diffusion of D through the PT inside surface oxide, not covered in this assessment,
3. Thermal Diffusion of H/D within the PT RJ based on Sorret's law,
4. Elastodiffusion of H/D within the PT RJ,
5. Concentration gradient driven diffusion of H/D within the PT RJ under Fick's law.

The geometry of ingress/diffusion for the PT RJ is illustrated in Figure 1, below.

Figure 1- Schematic of PT RJ Diffusion



Note that in the diffusion equations, the dimension in the circumferential direction, θ , is represented by y , where

$$y = r_m \theta$$

and r_m is the mean radius of the PT.

For this assessment, no quantitative analysis of through-wall (radial) diffusion and concentration differences has been performed..

The technical background on the above diffusion mechanisms, relevant to the analyses in this assessment, are presented below.

1. Electrochemical diffusion of H/D from the EF into the PT RJ based on Raoult's law

H/D, while in solution in steel, is at a higher electrochemical potential than when dissolved in zirconium, and therefore, will be driven by the electrochemical potential gradient, $\text{grad}(\mu)$, to diffuse from the EF to the PT, as predicted by Raoult's law:

$$\mathbf{J} = \frac{-DC}{RT} \nabla(\mu) \dots\dots\dots 1$$

Where J is the flux of H/D
 D is the diffusion coefficient
 C is the concentration

R is the universal gas constant
 T is the absolute temperature
 μ is the electrochemical potential of H/D in solution

In the case of radial (in the r direction) diffusion from the EF to the PT studied here, Equation 1 becomes:

$$\mathbf{J} = \frac{-DC}{RT} \frac{\partial \mu}{\partial r} \dots\dots\dots 2$$

2. Diffusion of H/D within the PT RJ in a Concentration Gradient based on Fick's law

In the event that local diffusion of H/D causes a local build up of H/D in an area of the PT, a concentration gradient will be established in the PT material. Fick's law states that the concentration gradient would drive the diffusion of H/D down the concentration gradient, i.e. atoms would migrate from the material with a higher concentration to the area with a lower concentration.

For a concentration gradient of grad (C), the flux in any direction due to Fick's diffusion is given by:

$$\mathbf{J} = -D \nabla (C) \dots\dots\dots 3$$

In the case of circumferential diffusion (in the θ direction) studied here, Equation 3 becomes

$$\mathbf{J} = -D \frac{\partial C}{\partial y} \dots\dots\dots 4a$$

In the two-dimensional case of axial and circumferential diffusion of Section 5.2.3,

$$\mathbf{J} = -D \left(\frac{\partial C}{\partial x} + \frac{\partial C}{\partial y} \right) \dots\dots\dots 4b$$

3. Thermal Diffusion of H/D within the PT RJ based on Sorret's law

When in solution inside the PT material, should H/D be exposed to a temperature gradient, grad (T), the H/D atoms will diffuse down the temperature gradient, as predicted by Soret's law:

$$\mathbf{J} = \frac{-DQC}{RT^2} \nabla (T) \dots\dots\dots 5$$

In Equation 5, Q is the activation energy for diffusion and T is the absolute temperature.

In the case of circumferential diffusion (in the θ direction) studied here, Equation 5 becomes

$$J = \frac{-DQC}{RT^2} \frac{\partial T}{\partial y} \dots\dots\dots 6$$

4. Elastodiffusion of H/D within the PT RJ

In the event of a hydrostatic stress gradient in the solvent material, H/D will undergo diffusion in the stress gradient, given by Equation 7.

$$J = - D S \Phi (V_H /RT) \frac{\partial \sigma_H}{\partial x} \dots\dots\dots 7$$

where J is the flux of H/D
 D is the diffusion coefficient
 Φ is the ratio of concentration to solubility
 V_H is the molar volume of D
 σ_H is hydrostatic stress given by:

$$\sigma_H = \Delta P = 1/3(\sigma_{11} + \sigma_{22} + \sigma_{33}) \dots\dots\dots 8$$

where σ₁₁, σ₂₂, and σ₃₃ are principal stresses in the axial, circumferential, and radial directions.

2.2 Understanding of H/D distribution Prior to 2021

In developing an understanding, and later, a physical model to predict H/D ingress and diffusion in the PT, consideration was given primarily to axial diffusion. It appears that radial diffusion was not considered to be significant issue. This could be attributed to the axisymmetric geometry for the PT and of the mechanisms responsible for H/D ingress into the PTs. For example, waterside corrosion of the inside of the PT, leading to D ingress at the PT inner surface could reasonably be expected to be the same around the circumference of the PT at given axial location.

In practise, it was determined that a small difference in [Heq] exists in the body of the PT at the top PT compared with the bottom. A typical example provided by Bruce Power is given below which shows that the [H/D] concentration at the top of the PT is higher than that at the bottom of the PT.

As a result, axial PT scrapes have almost entirely been performed at or near the 12 o'clock angular position at the top of the PT, which is very convenient for the retrieval of the scrape specimen.

Over the years, the H/D ingress models considered only ingress and axial diffusion, which was an entirely reasonable approach at the time. The focus on axial diffusion was manifested in numerous publications which always contained tables and plots of the axial distribution of Heq, and as a rule, never contained circumferential profiles. In the traditional plots of [Heq]

versus axial position, the understanding was that the [Heq] data point at a given axial position was the highest [Heq] at that position and was representative of the concentration at each point around the circumference of the PT.

Regarding the detection of [Heq] values exceeding 120 ppm in the Bruce PT RJs, the industry has been aware for many years of the possibility that [Heq] values could significantly exceed 120 ppm in the PT RJs. One of many examples is provided in Table 1, below, taken from Reference [1].

Table 1 – Predicted [Heq] Values at the PT Outlet RJ vs Axial Position and Time In-Service

Years in Service	Distance from the Outlet End of the PT		
	15 mm	80 mm	500 mm
	Hydrogen Equivalent Concentrations (ppm)		
15	130	67	33
20	177	70	40
25	224	72	47
30	270	79	54

It must be noted that the location of the maximum [Heq], where 120 ppm is predicted to be exceeded, is well within the PT RJ, in which:

1. Stresses in the PT RJ are compressive
2. Dispositionable flaws in the PT RJ are extremely unlikely.

2.3 Bruce Power’s Hypothesis for the Cause of Elevated Heq Measurements


The current theory held by Bruce Power is that the elevated [H/D] levels at the top of the PT due to the diffusion of H and D to a cold spot at the top of the PT from an adjacent region of the PT. There are several statements of this hypothesis in the Bruce Power submissions but the most demonstrative was found in CMD 21-H11.2A, which is reproduced as Figure 2, below

Figure 2
Slide 19 of Bruce Power Presentation of September 21, 2021

Understanding the Mechanism

- Higher hydrogen concentrations are encountered in some pressure tubes and are consistently found at top of tube in a narrow region of interest.
 - For affected pressure tubes, measurements in areas outside of the region of interest at top of the tube are significantly lower and within traditional model predictions.
- Hydrogen redistribution is occurring due to a temperature gradient at outlet ends.
 - Analysis has been completed based on recent results to understand this mechanism.

Elevated hydrogen concentrations are limited to a small portion of the pressure tube as determined through extensive scrape sampling and surveillance results.


19

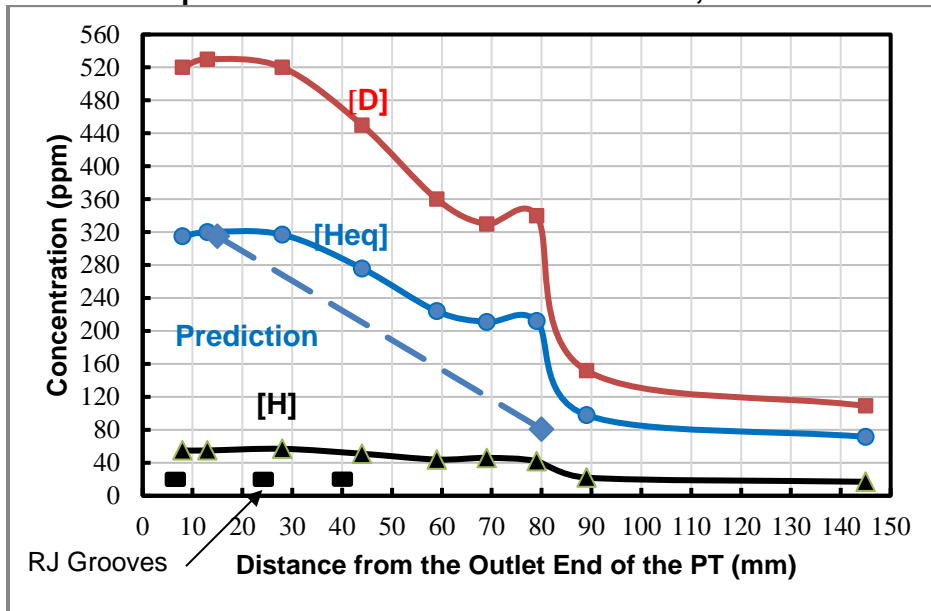
In addition to the thermal diffusion hypothesis, there is a secondary contention that the thermal diffusion is a redistribution process. The implication is that the total amount of H/D in the B6S13 outlet PT RJ is not abnormally high, but could be in the normal range.

The two hypotheses will be denoted as the thermal diffusion theory, and the H/D redistribution theory.

3. Initial Assessment of the B6S13 H/D concentration Data

Figure 3 presents a plot of H, D, and Heq concentration ([H], [D], [Heq]) measurements, for the outlet RJ in B6S13 versus distance from the outlet end of the PT. All the measurements are from the 12 o'clock position. The measurements were taken from Table A-2 in Attachment A of CMD21-M37-1.

Figure 3 – Axial [H], [D], and [Heq] Profiles at the Top of the Outlet PT RJ in B6S13 at 271,729 HH



A generic prediction of [Heq] from COG-94-509, Reference [1], is provided in Figure 3 for comparison. Although there is good agreement between the generic prediction and the measurement from B6S13 at the 15 mm location, [Heq] for B6S13 at the 80 mm location is severely underestimated by the generic model.

The shape of the axial Heq profile of Figure 3 is more consistent with the existence of a local source of H/D at the top of the PT than with thermal diffusion to the top of the PT. This is because the concentration profile in a thermal field will resemble the temperature profile, which would be wider and shallower than the concentration profiles of Figure 3.

Figure 3 appears to indicate the presence of a source of D and H ingress in a region at the top of the PT, ranging from 8 to 28 mm from the outlet end of the PT. That the concentration peak is limited to an axial region of the PT which is rolled into the EF implies that the peak is most reasonably attributable to diffusion from the EF into the section of the PT that is affected by the

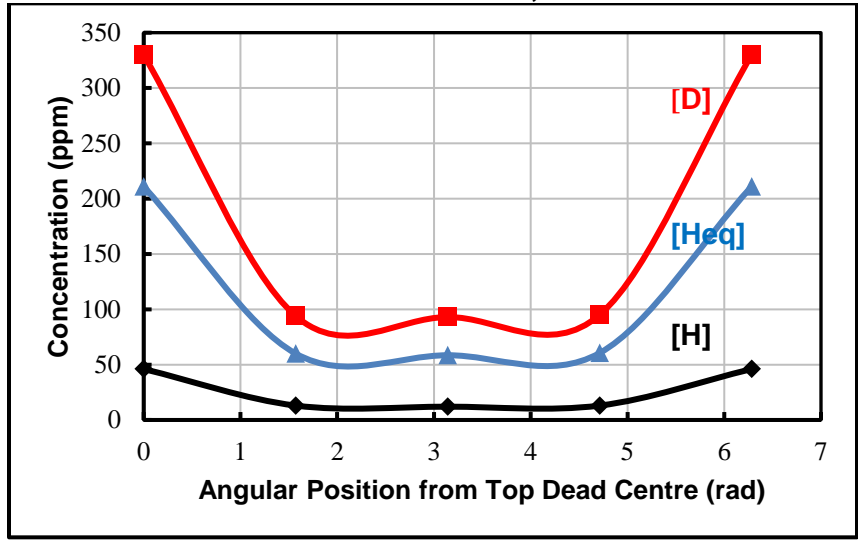
rolling of the PT into the EF. As shown in the figure, the peak of the [H] and [D] profiles coincides with location of the most outboard RJ groove.

This suggests the possible existence of a dominant source of ingress at the outboard groove, which could be explained by local cracking of the PT oxide layer at the groove during the RJ rolling process. The cracking and subsequent plastic deformation of the could form regions of direct contact of the EF and the PT, promoting ingress from the EF to the PT.

The observation of a higher concentration of D at the outer surface of the PT RJ than at the inner surface is consistent with the existence of an ingress source at the PT outer surface, more than likely electrochemical diffusion from the EF into the PT.

Figure 4 is a plot of the circumferential distribution of [H], [D], [Heq] at the BM for B6S13. As before, in the case of Figure 3, the shape of the circumferential distribution suggests the presence of an ingress mechanism at the top of the PT rather than a diffusion mechanism to drive H and D to the top of the PT. The circumferential concentration gradient intuitively appears to be too steep to have been created by the diffusion of H/D to the top of the PT RJ.

Figure 4
Circumferential Distribution of [H], [D], and [Heq] at the Outlet PT RJ of B6S13 at 271, 729 HH



Finally, the peak [D] value seen at 79 mm from the outlet end of the PT may be attributable to elastodiffusion from the area of residual compressive radial stresses in the PT RJ to the area of residual tensile circumferential stress inboard the BM.

4. Initial Assessment of the B3 Data

In the review of the B3 data, it was noted that B3F16 stood out among the sampled PTs because of noticeably high concentration measurements. [H] and [D] measurements versus distance from the outlet end of the PT are plotted in Figure 5.

It is seen in Figure 5 that the peak of the D concentration is very localised and the concentration gradient in the axial direction is very steep in comparison to the axial gradient for B6S13 in Figure 3. Intuitively, the axial concentration gradient is too steep to be associated with a thermal gradient in the PT, to a greater extent than is shown in the B6S13 concentration measurements.

To investigate the concentration gradient further, the circumferential [D] distributions for the outlet RJs of B6S13 and B3F16 were plotted in Figure 6.

Figure 5
[D] Measurements versus Distance from the Outlet End of the PT in B3F16 at 2 Circumferential Locations

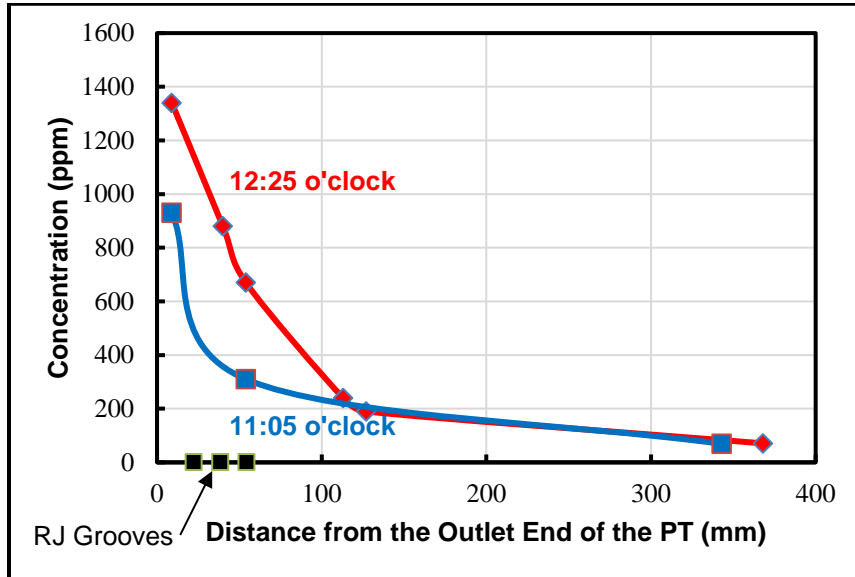
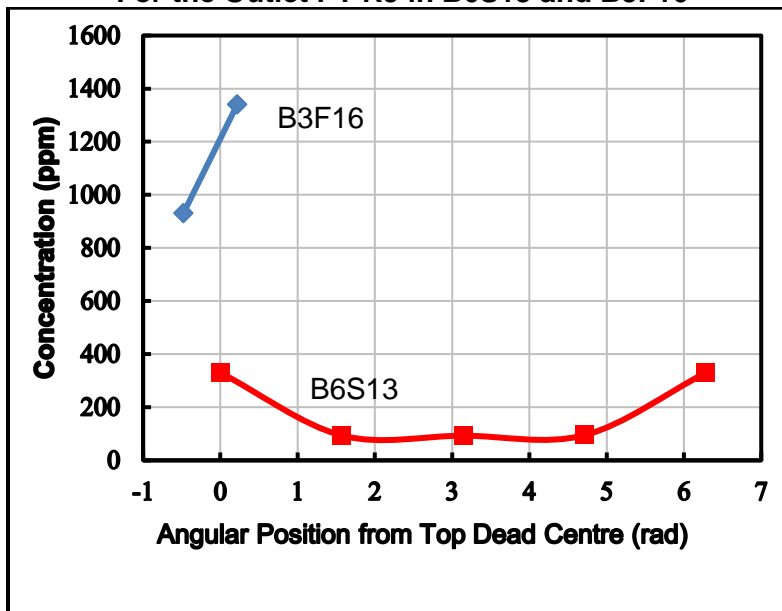


Figure 6
[D] Measurements versus Angular Position For the Outlet PT RJ in B6S13 and B3F16



The main point derived from the comparison of the B6S13 and the B3F16 measurements is that the two circumferential [D] profiles are significantly different, whereas only minor differences are expected in the operating temperature distributions at the PT outlets of the B6S13 and the B3F16. Therefore, the differences in the shapes and magnitudes of the concentration profiles of Figure 6 are more consistent with the existence of individual, PT-specific local sources of H/D at the top of the PT than with thermal diffusion to the top of the PT.

5. Analysis of the B6 Data

5.1 Test of Bruce Power's Hypotheses

Bruce Power's hypotheses were tested for B6S13 as documented in Sections 5.1.1 and 5.1.2. Section 5.2.1 covers a test of the thermal diffusion theory and Section 5.2.2 covers a test of the H/D redistribution theory.

5.1.1 Test of the Thermal Diffusion Theory - Prediction of the Circumferential Temperature Gradient required to Generate the H and D Concentration Gradients observed at the Outlet BM of B6S13

Considering the fixed moment in time at 271,729 HH corresponding to the concentration profile of Figure 4 and looking at the circumferential direction only, the Bruce Power hypothesis implies that the circumferential temperature gradient alone was driving H and D up the observed concentration gradient to the top of the PT. Under this condition, the magnitude of the observed circumferential concentration gradient can be used to estimate the minimum thermal gradient necessary to establish the concentration gradient.

Assuming a circumferential thermal gradient in the outlet PT RJ at the axial position of the BM, with the highest temperature along the horizontal axis of the PT and the lowest temperature at the top, circumferential thermal diffusion to the top of the PT would have occurred with a flux given by:

$$J = \frac{-DQC}{RT^2} \frac{\partial T}{\partial y} \dots\dots\dots 8$$

With time, the thermal flux would have generated a concentration gradient, with a higher concentration at the top of the tube, such as that observed in Figure 3.

Once established, the circumferential concentration gradient would have produced a flux from the top of the PT, in opposition to the thermal flux, given by:

$$J = -D \frac{\partial C}{\partial y} \dots\dots\dots 9$$

To establish and sustain the circumferential Heq profile observed in Figure 4, the instantaneous circumferential thermal flux to the top of the PT (Equation 8) would, at least,

have had to equal that generated by Fick's diffusion. Therefore, equating the fluxes in Equations 8 and 9 results in Equations 10a and 10b:

$$\frac{QC}{RT^2} \frac{\partial T}{\partial y} = \frac{\partial C}{\partial y} \dots\dots\dots 10a$$

$$\frac{\partial T}{\partial y} = \frac{RT^2}{QC} \frac{\partial C}{\partial y} \dots\dots\dots 10b$$

Equations 10a and 10b apply to all points along a streamline that defines the circumferential diffusion of H/D in the PT RJ.

Rather than directly extracting the concentration gradients for Figure 4, which has discontinuous [H] and [D] profiles for a lack of circumferential data, artificially smoothed profiles for [H] and [D] for the B6S13 outlet RJ were generated by fitting cosine functions to the concentration data of Figure 3.

The cosine functions for concentration in ppm versus angular position in radians are as follows:

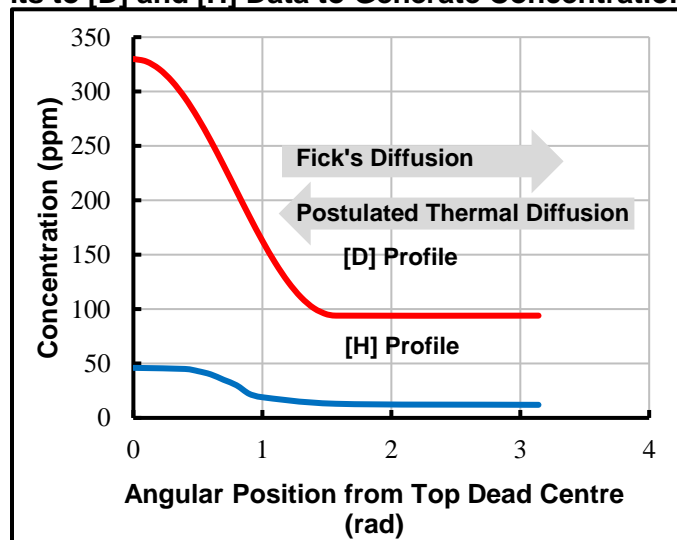
$$[D] = 0.5 \cdot (94 + 330) + 0.5 \cdot (330 - 94) \cdot \cos(2\theta) \dots\dots\dots 11$$

$$[H] = 0.5 \cdot (13 + 46) + 0.5 \cdot (46 - 13) \cdot \cos(2\theta) \dots\dots\dots 12$$

Although the fitted profiles will not be an exact reproduction of the actual profiles at the outlet BM, they are appropriate for the purposes of the temperature gradient analysis.

The smoothed [H] and [D] profiles are presented in Figure 7. The [D] and [H] concentration profiles and gradients for which $\frac{\partial T}{\partial y}$ were calculated, are presented in Figure 8.

Figure 7
Curve Fits to [D] and [H] Data to Generate Concentration Profiles



Equation 10b was used to predict the minimum temperature gradients at points along the circumferential concentration profile that would have been necessary to create the concentration gradients observed at the outlet BM of B6S13, assuming no other driving forces for diffusion in the circumferential direction, such as a circumferential stress gradient. At the BM, no circumferential elastodiffusion is considered to be a valid assumption because the residual circumferential stresses from the rolling process are considered to be uniform around the circumference of the RJ.

It should be noted that the activation energy in Equation 10b is subject to considerable variability. Various values for Q have been published over the years, as indicated in the Table below, extracted from Reference [2].

Table 1 – Parameters for Coefficient of Diffusion Relationships for Hydrogen (Protium)

Model		D_0	Q	
		(m^2/s)	(J/mol)	
[H] Sawatzky [1]		1.17E-07	33600	
[H] Léger [2][3]		4.10E-07	38400	
[H] Skinner [4]	PNGS	Axial	2.38E-07	35121
	DNGS	T1/S1	4.88E-07	41103
	DNGS	T1/S15	4.03E-07	40717
	DNGS	T2	1.37E-07	34445
	DNGS	T342	1.52E-07	34252
[H] Khatamian (longitudinal) [5]		3.69E-07	39007	

Subsequent research into hydrogen activation energy revealed that significantly higher values had been published in Molecular Dynamics Study of Hydrogen in α -Zirconium Reference [3], which gave an activation energy of 11.3 kcal/mol or 47297 J/mol.

Therefore, to account for the possible variability in activation energy values in Equation 10b, two analysis cases were considered: the first with Q = 47279 J/mol and the second with Q = 33600 J/mol as per Sawatzky from the Table above.

The analysis using Equation 10b was executed as follows:

1. The [H] and [D] versus Θ profiles, depicted in Figure 7, were differentiated with respect Θ to obtain $\partial C/\partial\theta$ vs Θ ,
2. The integrated average values for $\partial C/\partial\theta$ for the H and D profiles were calculated and were converted to average integrated values for $\partial C/\partial y$, given in Table 2,
3. Equation 10b was used to calculate the average integrated $\partial T/\partial y$ value from which the temperature difference from the side to the top of the PT outlet RJ was found,
4. To create the profile of the temperature required to sustain the concentration gradients observed in B6S13, for each value of $\partial C/\partial\theta$, $\partial T/\partial\theta$ was calculated using Equation 10b for the H and D profiles, a sine function was fitted to $\partial T/\partial\theta$ versus θ , and the sine function was integrated with respect to θ to obtain T(θ).

Figure 8 presents plots of the concentration gradient and concentration versus Θ for the PT outlet RJ of B6S13, from Step 1.

Figure 8
H and D Concentrations and Concentration Gradients versus Θ

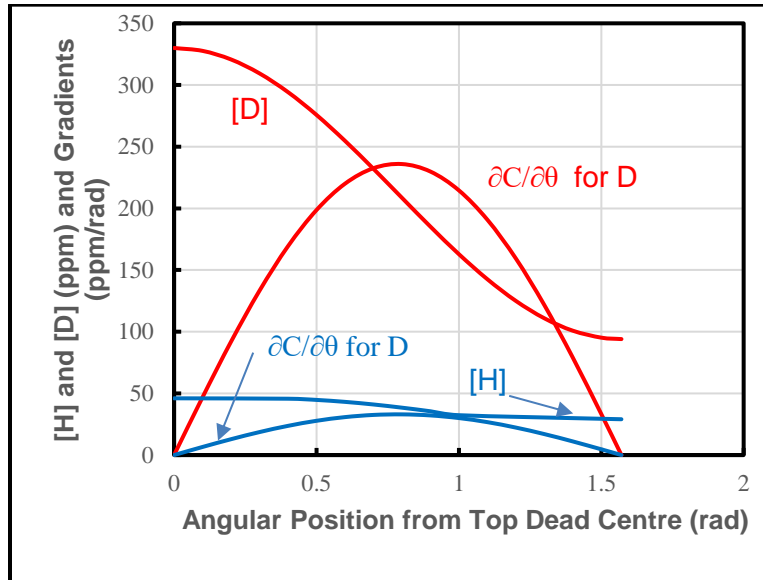


Table 2
Integrated Average [H] and [D] Gradients From Cosine Concentration Function

Atom	Concentration Gradient	
	$\partial c/\partial \theta$	$\partial c/\partial y$
	(ppm/rad)	(ppm/m)
H	19	358.8
D	139	2565.6

A summary of the temperature gradient analyses is presented in Tables 3 and 4, below. Table 3 is for the diffusion of H and Table 4 is for the diffusion of D. Note that the temperature and concentration values and the calculated concentration gradients in Tables 3 and 4 are for the solution point at $\Theta = 0.8$ radians. Note that Case 1 in Tables 3 and 4 is for the high value of Q and Case 2 is for the low value.

Table 3
Prediction of the Temperature Gradients Required to Generate the H Concentration Gradients of Table 2

Case	r_m	$\partial c/\partial y$	Q	R	T	T	C	$\partial T/\partial y$	$\partial T/\partial \theta$	$\Delta \theta$	ΔT	$T_{0 \text{ rad}}$
	(m)	(ppm/m)	(J/mol)	(JK ⁻¹ mol ⁻¹)	(°C)	(K)	(ppm)	(°C/m)	(°C/rad)	(rad)	(°C)	(°C)
1	0.054	358.8	47279	8.313	256.3	529.5	29	609.3	32.928	1.571	51.7	204.6
2	0.054	358.8	33600	8.313	239.7	512.9	29	804.5	43.474	1.571	68.3	171.4

Table 4
Prediction of the Temperature Gradient Required to
Generate the D Concentration Gradient of Table 2

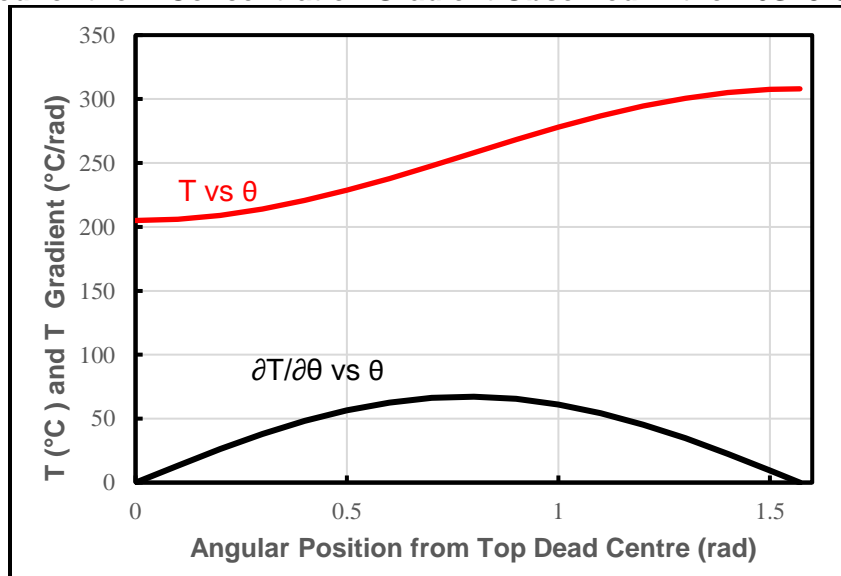
Case	r_m	$\partial c/\partial y$	Q	R	T	T	C	$\partial T/\partial y$	$\partial T/\partial \theta$	$\Delta \theta$	ΔT	$T_{0 \text{ rad}}$
	(m)	(ppm/m)	(J/mol)	($\text{JK}^{-1}\text{mol}^{-1}$)	($^{\circ}\text{C}$)	(K)	(ppm)	($^{\circ}\text{C}/\text{m}$)	($^{\circ}\text{C}/\text{rad}$)	(rad)	($^{\circ}\text{C}$)	($^{\circ}\text{C}$)
1	0.054	2565.6	47279	8.313	256.5	529.7	209	606.8	32.79	1.571	51.5	205.0
2	0.054	2565.6	33600	8.313	240	513.2	209	801.5	43.309	1.571	68.0	172.0

Table 5
Nomenclature for Tables 3 and 4

r_m	Mean Radius of the B6S13 Outlet PT RJ
$\partial c/\partial y$	Concentration gradient
Q	Activation energy for H in Zr
R	Gas constant
T	Absolute temperature at solution point
C	Local concentration at solution point
$\partial T/\partial \theta$	Temperature gradient
$\Delta \theta$	Change in angular position along diffusion path
ΔT	Change in temperature along diffusion path
$T_{0 \text{ rad}}$	Temperature at 0 radians resulting from ΔT

A graphical summary of the entire circumferential temperature profile prediction, presented above, is provided in Figure 9, below.

Figure 9
Predicted Temperature and Temperature Gradient
Required for the D Concentration Gradient Observed in the B6S13 Outlet RJ



The predicted temperature profile of Figure 9 is for Case 1, which gives the highest temperature at the top of the PT, which represents the most favourable result in support of the thermal diffusion theory.

As seen Figure 9, it is predicted that a considerable circumferential temperature gradient would have had to be in existence at the outlet BM of B6F13 to create the circumferential concentration gradients observed. The resulting temperatures at the top of the PT, $T_{0\text{ rad}}$, appear to be reasonable, in comparison to the channel outlet temperature.

Having predicted the required temperature gradients, the next step in the assessment was to determine the likelihood that the predicted temperature gradients actually existed in B6S13, as follows.

It was assumed that the channel outlet temperature for B6F13 at 271,729 HH was 308 °C. In all of the previous PT fitness-for-service assessments in all CANDU reactors, flaws near or at the outlet BM were assigned temperatures based on channel outlet temperatures. The heat transfer in the fuel channel during normal reactor operation is such that the PT temperature is dominated by the temperature of the coolant.

In principal, for a fuel channel in the design basis condition, there is no mechanism for the creation of a significant cold spot anywhere in the PT outlet RJ since the outlet end of the PT is exposed to coolant at the channel outlet temperature.

In the Bruce Power documents that were reviewed, there are references to a cold spot at the top of the PT but no specific information is provided.

For the purpose of this assessment, with no details of the temperature gradient given in the Bruce Power submissions reviewed, it was assumed that the temperature gradient in question would have been produced by flow by-pass as a result of diametral creep of the PT.

As a result of PT diametral creep, a space will develop between the top of the fuel bundle and the top of the PT with time in-service, centred at bundles 8 – 10, depending on the fuel channel and station. Flow by-pass involves the diversion of about 35% of the flow, at maximum, into the space above the bundle, instead of flowing through the subchannels inside the bundle.

Consequently, with flow by-pass, less heat will be transferred to the flow at the top of the PT compared with the rest of the flow in the PT, leading to lower temperatures at the top of the PT.

Figure 10 presents a predicted coolant temperature in a PT with flow by-pass, based on the analysis methods of Reference [4].

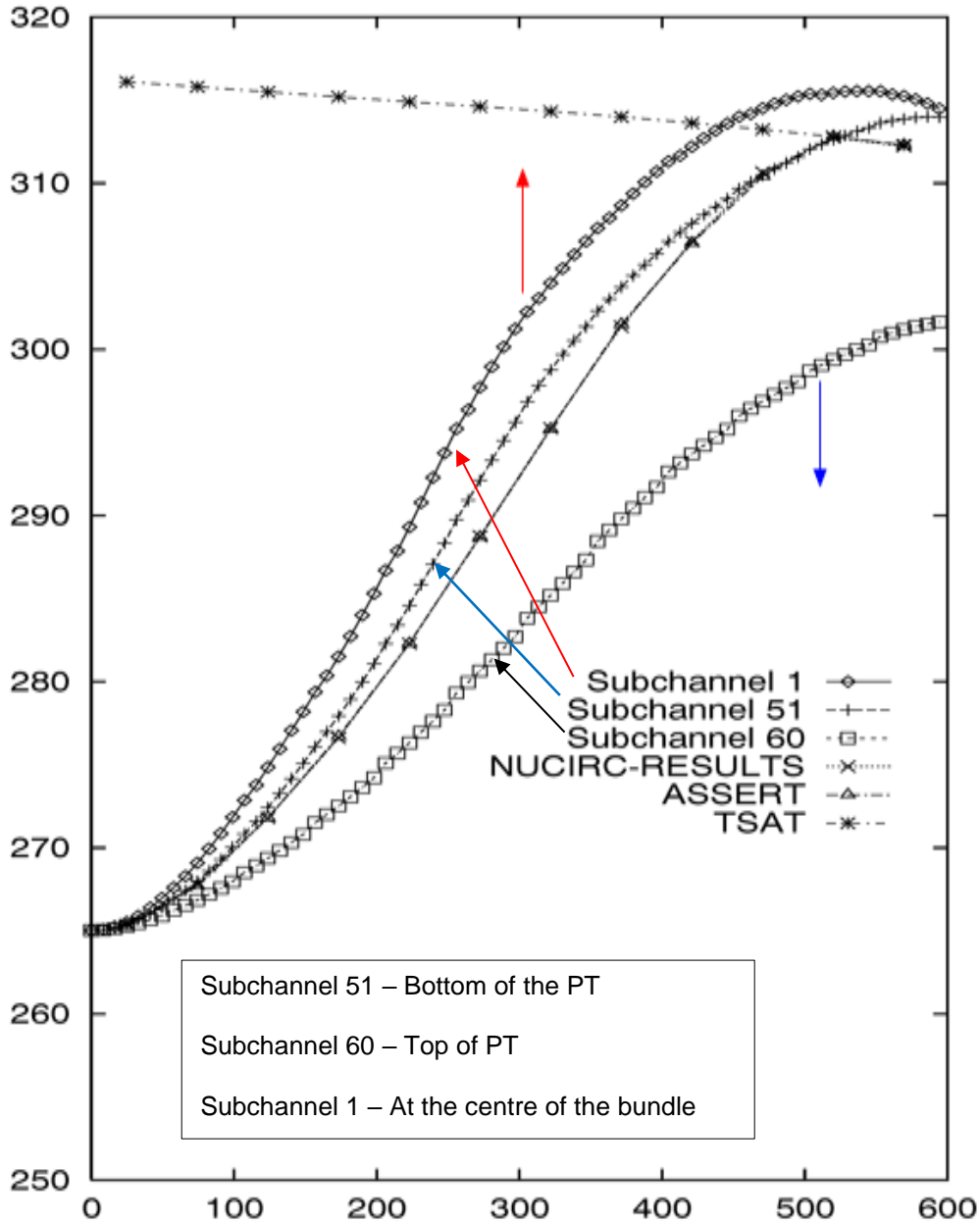
The temperatures presented in Figure 10 were extracted from ASSERT computations of the temperatures of the coolant in the flow subchannels in a crept PT, noting that subchannel 60 is at the top of the PT where flow bypass occurs and subchannel 51 is at the bottom of the PT.

For this assessment it was assumed that the temperature of PT would equal that of the coolant in contact with it and that the temperature at the bottom of the PT would equal that the 3 and 9 o'clock positions. The later assumption is considered reasonable since the flow distributions at the 3, 6, and 9 o'clock positions would not be significantly altered by PT diametral creep.

Figure 10 indicates that there would be a 12 °C difference between the top and side of the PT at the outlet due to flow bypass or 6 °C over an angle of 1.517 radians, for a temperature gradient of 8

°C/rad. From Tables 3 and 4, it is seen that, at minimum, a circumferential temperature difference of 52 °C from 0 to $\pi/2$ radians would be required to generate the concentration gradients in question.

Figure 10
Plot of Coolant Temperatures in a PT with Flow Bypass



The figure shows that in a crept PT, the coolant temperature is approximately 12 °C lower at the top of the PT outlet than at bottom of the PT outlet. From the geometry of the fuel bundle and the crept PT, it was assumed that the coolant temperature at both sides of the PT would equal that at the bottom, so that the coolant temperature would increase around the circumference of the PT by 12 °C from 0 radians (Top Dead Centre) to $\pi/2$ radians (3 o'clock). The thermal hydraulics of the PT are such that the PT temperature is assumed to be the same as coolant temperature.

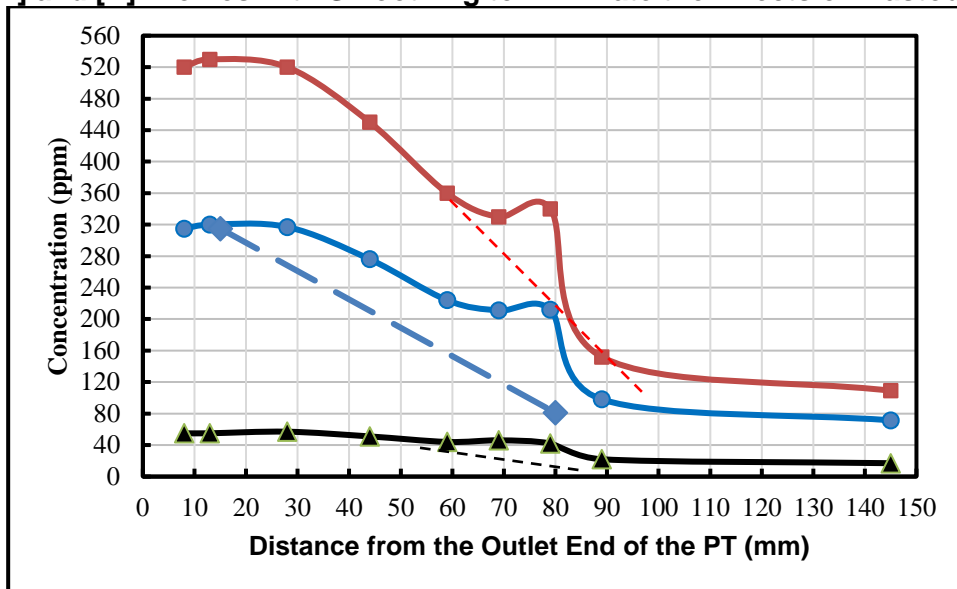
In summary, the assessment of Tables 3 and 4 indicates that the minimum top-to-side temperature difference required to generate the observed concentration gradients in the B6S13 is 52 °C, compared with an expected temperature difference of 12 °C, from Figure 10.

Given the approximate nature of the calculations in Table 3 and 4, the above results are inconclusive, which led to an attempt to refine the calculations in Section 5.2.1.1

5.1.1.1 Refinement to Calculations of the Circumferential Temperature Gradient required to Generate the H and D Concentration Gradients observed at the Outlet BM of B6S13

Figure 11 is a reproduction of Figure 2, with dashed lines from 60 to 90 mm representing smoothing of the profiles by removing the local peak at 79 mm. The local peak is assumed to be due to elastodiffusion of H and D to the region of tensile hoop stress just inboard the BM. The smoothing of the the [H] and [D] profiles, by removing the peaks, represents the [H] and [D] profiles that would occur purely by thermal diffusion.

Figure 11
Axial [H] and [D] Profiles with Smoothing to Eliminate the Effects of Elastodiffusion



The smoothed profiles can then be used to investigate whether thermal diffusion alone could have generated the concentration profiles observed in B6S13, which is a refinement of the calculations presented in Tables 3 and 4, as follows.

From Figure 11, it is estimated that with smoothing of the profiles, the [H] and [D] values at the top of the PT would be reduced from 46 to 30 ppm for H and from 330 to 280 ppm for D. With smoothing, the resulting circumferential concentration data is shown in Figure 12.

Figure 12
Derived Circumferential Concentration Profiles from
Smoothing (No Elastodiffusion) of the Axial Profiles of Figure 9

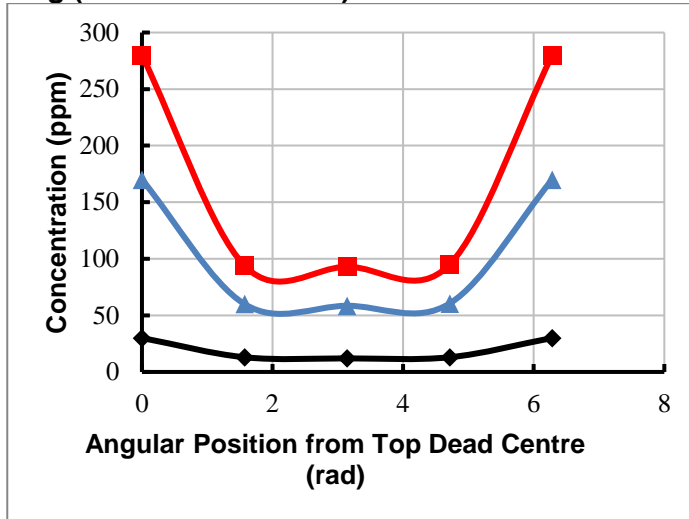
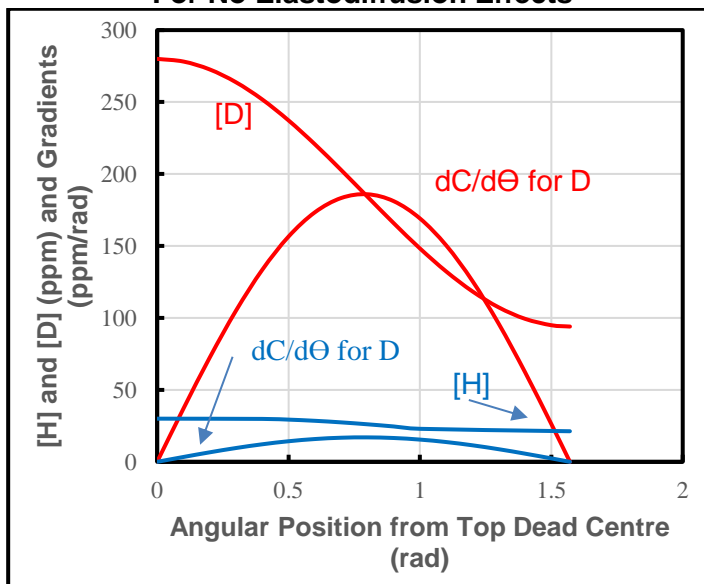


Figure 13, produced using the same procedures as described in Section 5.2.1, gives the fitted cosine functions for the H and D circumferential profiles and the fitted sine functions for the [H] and [D] gradients. It can be noted that the [D] profile in Figure 13 is lower than that in Figure 8.

Figure 13
H and D Concentrations and Concentration Gradients versus Θ
For No Elastodiffusion Effects



The analyses summarised in Tables 3 and 4 were repeated for no elastodiffusion and were detailed in Tables 6, 7, and 8.

Table 6
Average Circumferential Concentration Gradient from Concentration Cosine Functions

Atom	$\partial c/\partial\theta$	r_m	$\partial c/\partial y$
		(m)	(ppm/m)
H	10	0.0540	184.8
D	109	0.0540	2022.1

Table 7
Prediction of the Temperature Gradients Required to
Generate the H Concentration Gradients of Table 6 Removing Elastodiffusion Effects

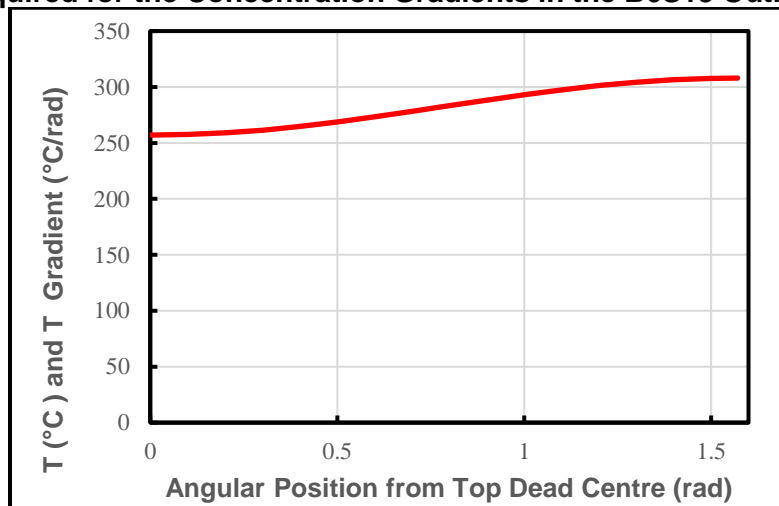
Case	r_m	$\partial c/\partial y$	Q	R	T	T	C	$\partial T/\partial y$	$\partial T/\partial\theta$	$\Delta\theta$	ΔT	$T_{0 \text{ rad}}$
	(m)	(ppm/m)	(J/mol)	(JK ⁻¹ mol ⁻¹)	(°C)	(K)	(ppm)	(°C/m)	(°C/rad)	(rad)	(°C)	(°C)
1	0.054	184.8	47279	8.313	287.6	560.8	21	480.8	25.981	1.571	40.8	267.2
2	0.054	184.8	33600	8.313	280.1	553.2	21	658.4	35.581	1.571	55.9	252.1

Table 8
Prediction of the Temperature Gradients Required to
Generate the D Concentration Gradients of Table 6 Removing Elastodiffusion Effects

Case	r_m	$\partial c/\partial y$	Q	R	T	T	C	$\partial T/\partial y$	$\partial T/\partial\theta$	$\Delta\theta$	ΔT	$T_{0 \text{ rad}}$
	(m)	(ppm/m)	(J/mol)	(JK ⁻¹ mol ⁻¹)	(°C)	(K)	(ppm)	(°C/m)	(°C/rad)	(rad)	(°C)	(°C)
1	0.054	2022.1	47279	8.313	282.7	555.9	184	596.1	32.211	1.571	50.6	257.4
2	0.054	2022.1	33600	8.313	273.6	546.7	184	811.4	43.845	1.571	68.9	239.1

Lastly, the predicted temperature gradient and temperature profile, required to generate the circumferential [D] profile of Figure 11, are presented in Figure 14. It is seen that smoothing the circumferential D concentration profile did produce a noticeable reduction in the temperature difference required to generate the [D] profile of Figure 11.

Figure 14
Predicted Circumferential Temperature Profile
Required for the Concentration Gradients in the B6S13 Outlet RJ



Specifically, examining the temperature profile predictions for the diffusion of D of Tables 3 and 8, the temperature at the top of the PT outlet would have to have been 257 °C, excluding elastodiffusion, and 205 °C including elastodiffusion.

At this stage, it was not known if the attempt to refine the predictions of Section 5.1.1, with the calculations in Section 5.1.1.1, will advance the cause of conclusively determining the validity of Bruce Power's diffusion thermal theory.

5.1.2 Test of the H/D Redistribution Theory – Estimation of the H/D Content of the B6S13 Outlet PT RJ

To test the H/D redistribution theory, the following analyses were performed:

1. The average [Heq] at the outlet BM of B6S13 at 271729 HH was predicted and compared with the expected typical value, as summarized in 5.1.2.1.
2. The total D content in the B6S13 outlet PT RJ at 271729 HH was predicted and compared with the expected typical value, as summarized in 5.1.2.2.

5.1.2.1 Average [Heq] at the Outlet BM

The average [Heq] value was calculated along the following lines.

1. A simulated [Heq] profile was generated at the BM from 0 to 3.142 rad, which is depicted in Figure 6.
2. A polynomial curve fit was generated to the [Heq] profile from 0 to 1 rad.
3. The [Heq] profile from 1 rad to 3.142 was modeled as a series of straight lines,
4. The [Heq] profiles were integrated with respect to angular position from 0 to 2π radians to find the average [Heq] at the BM over the full circumference of the PT.

Following the procedure above, the average [Heq] at the BM was found to be 99.1 ppm.

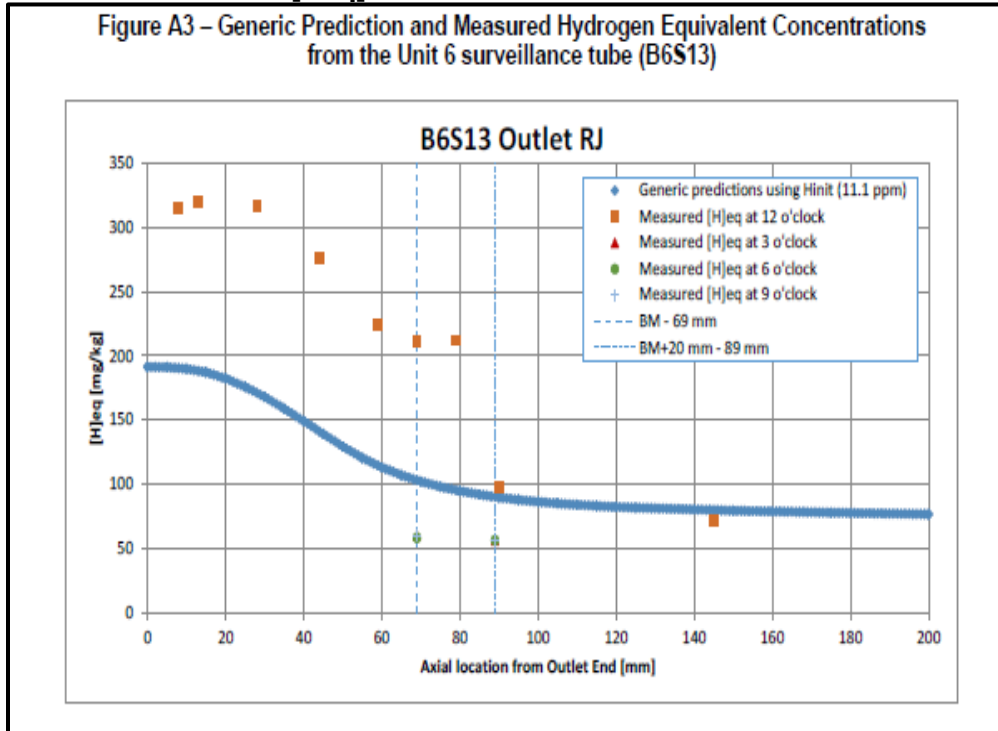
The above value should be compared with the mean [Heq] measured or predicted for PTs that demonstrate normal H/D ingress behaviour, without elevated concentrations at the top of the PT.

In the absence of readily available data of this type, Figure 13, reproduced from CMD 21-H11.2B, provides a convenient approximation of the typical [Heq] at the outlet BM.

From Figure 13, the typical [Heq] value at the outlet BM for a Bruce Unit 6 PT is approximately 90 ppm, which is in reasonable agreement with the value calculated here.

The agreement between the calculated average [Heq] value and that given in Figure 15 provides some confirmation of Bruce Powers hydrogen distribution theory.

Figure 15
[Heq] Measurements for B6S13



5.1.2.2 Total D Content in the Outlet PT RJ for B6S15

The total D in the outlet PT RJ for B6S15 was calculated along the following lines.

1. The axial [D] profile for the top of the PT was discretized into 6 axial stations.
2. For each axial station, a circumferential [D] distribution was generated.
3. The average [D] in ppm by mass in each axial station was calculated by integration of the [D] profile with respect to angular position from 0 to 2π radians.
4. Knowing the ppm of D in each axial station of the PT and the mass of each station, the total mass of D in the PT RJ was calculated.

Following the above steps, it was predicted that the outlet PT RJ of B6S13 contains 198 mg of D, noting that the PT RJ is assumed to extend from the outlet end of the PT to 145 mm inboard the outlet end of the PT.

Figure 14, below shows that the outlet PT RJ contains approximately 122 mg of D, as compared with 198 ppm from this assessment. The source of this discrepancy was not investigated. However, from Figure 9, the conclusion is that the B6S13 outlet PT RJ did not absorb an abnormal amount of D. As in 5.1.2.1, the calculated amount of D in the PT RJ may support the hydrogen redistribution theory.

Figure 16
Plot of RJ D Uptake vs Time

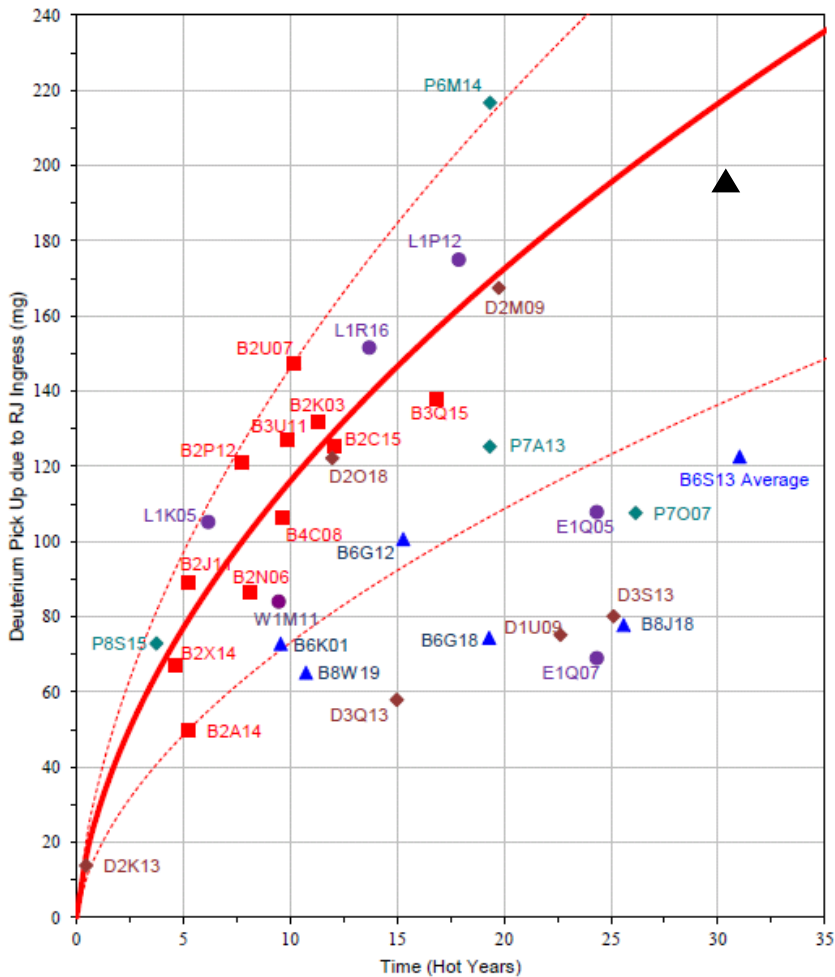


Figure 17 Mass of deuterium in mg picked up at the outlet rolled joint as a function of time for Bruce A (red squares), CANDU 6 (purple circles), Darlington (maroon diamonds), Pickering B (teal diamonds) and Bruce B (blue triangles) outlets. The solid curves are the best fit, assuming a declining ingress rate and the dashed curves represent upper and lower bounds to the Bruce A ex-service pressure tube data.

5.2 Alternative Theory for the Cause of Elevated [H/D] at the Top of the PT

5.2.1 Proposed Alternative Hypothesis

As outlined previously, there are several indications of the existence of a local source of H/D at the top of the PT outlet RJ in B6S13 and B3F16. The resulting hypothesis is that the elevated H and D concentrations measured at the top of the PT RJ are due to the electrochemical diffusion of H and D from the EF, through openings in the oxide layer of the PT that was rolled into the EF grooves. Under the local D source hypothesis, the D would enter a local volume the top of the PT RJ, cause an elevated local accumulation of D, as shown in Figures 2 and 3, and, by Fick's diffusion, D would exit the local volume into the rest of the PT.

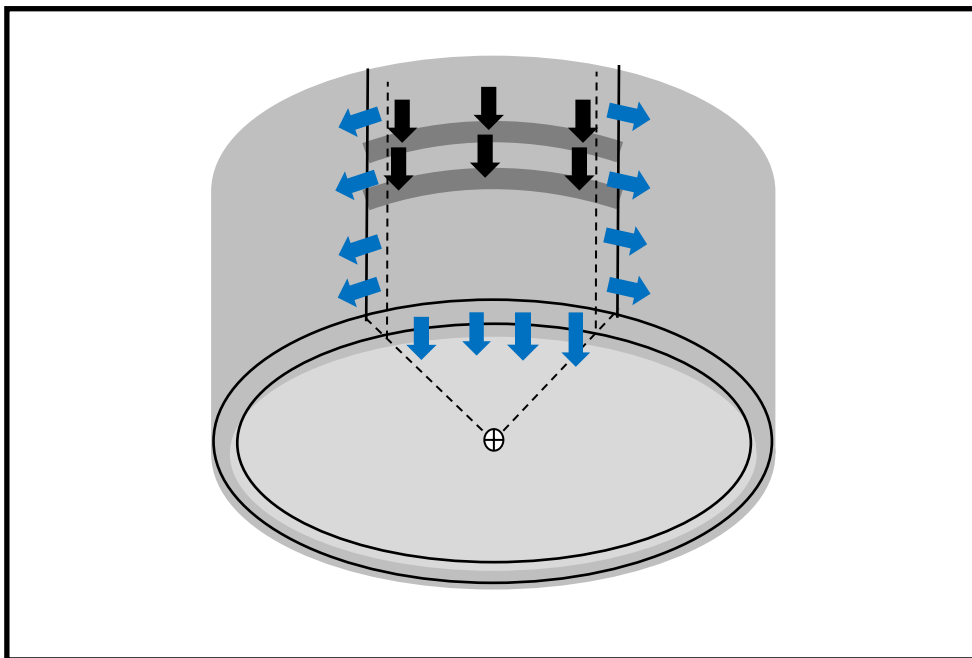
To test the hypothesis, predictions of the electrochemical mass flow rate of D from openings in the PT oxide layer into a local volume at the top of the PT outlet RJ in B6S13 were generated. The mass flow rate was then compared to the mass flow rate predicted by Fick's diffusion out of the of the local volume. The rationale for testing the hypothesis is as follows:

1. If the predicted ingress mass flow rate into the local volume is lower than the predicted exit mass flow rate, the hypothesis is false,
2. If the difference between the ingress and exit mass flow rates is consistent with the D profiles of Figures 2 and 3, then the hypothesis could be true.

5.2.2 Predicted Mass Flow Rate of D into the Local Volume by Electrochemical Diffusion

Figure 17 depicts the diffusion scenario that is being postulated. The figure illustrates the postulated flow of D from the EF into the local volume through the deformed PT material at the grooves and the flow of D out of the local volume. The local volume at the top of the PT was designed to contain the peak of the axial [D] profile and the boundaries were selected to line up with specific points in the measured [D] profiles where gradients were calculated. The local volume starts at the outlet end of the PT and extends 28 mm inboard, and covers an arc at the top of the PT from -0.8 to 0.8 radians. There are two RJ grooves within the local volume.

Figure 17
 Illustration of the Local Volume for the Prediction of D Diffusion
 From the Postulated Electrochemical Source at the RJ Groove



The depicted volume is at the top of the outlet end of the PT RJ in B6S13, with dimensions given in Appendix 1. The black arrows depict the postulated D deingress into the top of the PT. The blue arrows depict the Fick's diffusion that would occur in response to [D] concentration gradient.

Figure 18 depicts the postulated local damage to the PT oxide layer at which direct contact of the PT material with the oxide layer on the EF is expected to have occurred.

Figure 18
Postulated Areas of Bare PT Material Contact with the EF Grooves

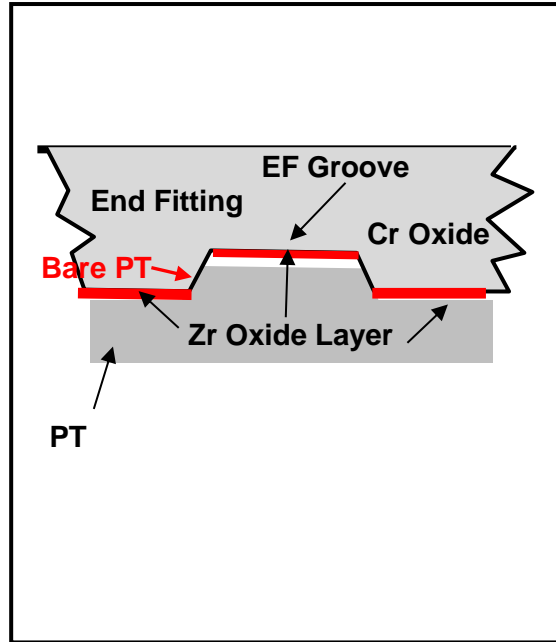


Figure 18 depicts the postulated damage to the PT oxide layer and the creation of areas of direct contact of the bare PT material with the oxide layer of the EF groove. It is expected that as the PT material is extruded into the EF groove, the corners of the groove will penetrate into the PT material and generate a new surface, in intimate contact with the EF groove. The contact of the EF surface with the bare surface of the PT results in a galvanic couple between the PT and the EF which is moderated by the chromium oxide layer on the EF. It is assumed here that the oxide layer survived the RJ rolling process and would act as a barrier to diffusion from the EF to the PT through the areas of intimate contact of the PT with the EF, described above.

At the contact surface of the PT and the EF RJs, some damage of both oxide layers is expected due to the rolling of the PT into the EF, but general damage is not definitive. For this assessment, it is expected that damage to the oxide layer on the PT would be localized at the grooves. Specifically, it is assumed that the corners of the EF groove would have penetrated into the PT RJ material creating areas of direct contact of the bare PT material with the oxide layer of the EF, as described in the caption to Figure 18. Under this assumption, electrochemical diffusion of H/D from the EF to the PT would have occurred through the small contact area of the bare PT material with the EF.

Details of the electrochemical diffusion analysis are presented in A1.2 of Appendix 1 and a summary of the analysis is presented below.

The analysis was started with a prediction of the D electrochemical flux using Equation 1. Temporarily ignoring the permeability of the chromium oxide layer on the outside of the EF groove, the electrochemical potential difference between the D in the EF and in the PT would have provided a very strong driving force for diffusion into the PT, as seen in Table A1-5. Realistically, the chromium oxide layer would have significantly reduced the D flux, but an exact calculation of the permeability of the oxide layer is beyond the scope of this work. Instead, an estimate of the D flux through the chromium oxide layer, due only to electrochemical driving forces, was taken from Reference [5] as $2.00E-05 \text{ mol m}^2 \text{ s}^{-1}$ or $4.02 \times 10^{-8} \text{ kg m}^{-2} \text{ s}^{-1}$, as seen in Table A1-6. For an area

of contact of the bare PT with the EF, estimated as 0.000226 m^2 , (see Appendix 1) the D mass flow rate into the local volume was predicted to be $9.481\text{E-}12 \text{ kg s}^{-1}$.

As a further refinement, detailed in Appendix 1, it is expected that the bare areas of the PT material in contact with the EF would have been under compressive stresses during reactor operation, because of differential thermal expansion of the PT material in the groove, relative to the groove in the EF, (see Table A1-7a). As a result, there would be a stress gradient in the region of bare contact of the PT with the EF groove, causing some diffusion of D back into the EF. The elastodiffusion calculations are covered in Tables A1-7a, A1-7b, and A1-7c. It was found that the estimated D flux from the PT/EF contact face back into the bulk material of the EF, was $4.03\text{E-}11 \text{ kg m}^{-2} \text{ s}^{-1}$, which is insignificant compared to the mass flow generated by the other diffusion mechanisms.

The final step in the analysis, the prediction of D mass flow rates from the postulated electrochemical source, is detailed in Table A1-8.

From the table, the total mass flow rate of D into the local volume, through the postulated bare areas of the PT material at the RJ grooves, was estimated to be $9.471\text{E-}12 \text{ kg s}^{-1}$.

5.2.3 Predicted Mass Flow Rate of D out the Local Volume by Fick's Diffusion

As detailed in Appendix 1, Fick's axial and circumferential diffusion fluxes for D out of the local volume shown in Figure 17 were calculated using Equation 4b. The resultant instantaneous mass flow rate of D out of the local volume was estimated as $1.217\text{E-}12 \text{ kg s}^{-1}$, specifically at 271,729 HH, as given in Table A1-8.

6. Discussion of Results

The results of Section 5.1 are discussed in Section 6.1. The results of Section 5.2 are discussed in Section 6.2.

6.1 Results from Section 5.1

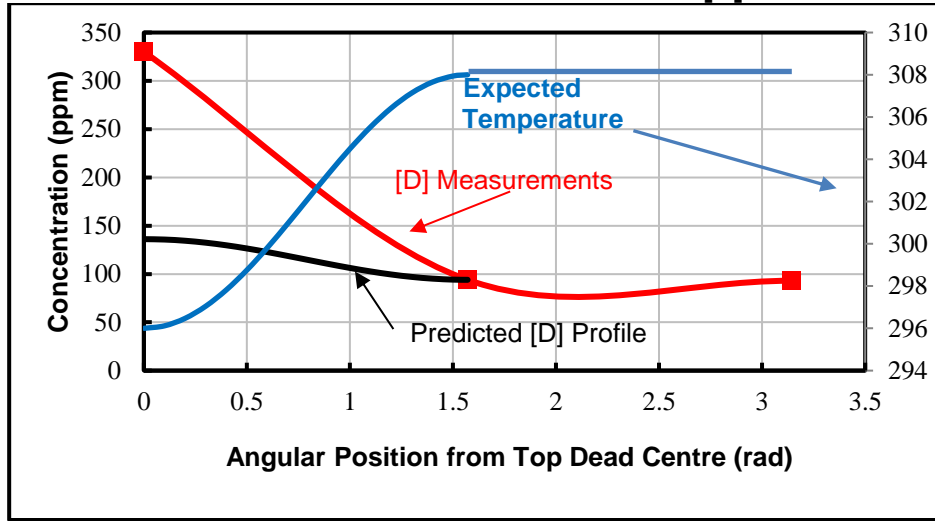
The test of Bruce Power's thermal diffusion theory in Section 5.1.1 produced more definite results than the test of the redistribution theory in Section 5.1.2.

Basically, the results of the diffusion analysis of Section 5.1.1 indicate that the expected thermal gradient during operation would have not been sufficient to cause the H/D concentration gradients measured in the outlet PT RJ of B6S13.

To illustrate that point, the required operating circumferential temperature profile to generate the H/D concentrations observed in B6S13 were compared with the expected temperature profiles. An alternative presentation is provided below, in Figure 19. In the Figure, the expected circumferential temperature profile (based on Figure 10) and the resultant predicted D concentration profile are plotted for comparison with the [D] measurements from the PT outlet RJ of B6S13.

Figure 19 shows that the expected circumferential temperature profile, shown in black, could have resulted in some diffusion to the top of the PT profile but the thermal diffusion could not have generated the observed [D] profile, shown in red.

Figure 19
Expected Circumferential Temperature & Predicted [D] Profiles
For the B6S13 Outlet RJ versus Measured [D] Profile



6.2 Results from Section 5.2

As a preamble, it should be recognized and acknowledged that the analyses are based on simple closed-form solutions of limited accuracy. In the industry, such approximate methods would be used in preliminary analyses and for QA verification purposes but H/D diffusion analyses for actual fitness-for-service assessments would use standard industry computation tools such as H3DMAP.

Therefore, the diffusion analyses of 5.2.2 and 5.2.3 are approximate and are only sufficient for indicating whether or not the alternative hypothesis for elevated [H/D] at the top of the PT from 5.2.1 is reasonable. Another point to be noted is that the calculations were not subject to QA verification as per standard industry practices.

From 5.2.2 and 5.2.3, in the B6S13 outlet PT RJ, the predicted mass flow of D into the local volume, $9.471\text{E-}12 \text{ kg s}^{-1}$, is more than sufficient to sustain the observed H and D concentration gradients, which indicate an instantaneous mass flow of D out of the local volume at a rate of $1.217\text{E-}12 \text{ kg s}^{-1}$, specifically at 271,729 HH. In reality, it appears that the D mass flow rate into the PT is significantly overestimated, probably because the H and D concentration gradient across the chromium oxide layer on the EF was not properly accounted for in the electrochemical diffusion analysis.

Regardless, the assessments of Sections 5.2.2 and 5.2.3 indicate that the physics of electrochemical diffusion through an area of intimate PT-EF contact, as postulated in 5.2.1, would have been sufficient to create the H and D concentration profiles depicted in Figures 2 and 3.

In CMD22-M37, it was stated that the outer surface of the outlet PT RJ in B6S13 was found to contain over 400 ppm [Heq] while the inner surface was found to be below 50 ppm [Heq]. This observation is more consistent with electrochemical diffusion of H and D from the EF than thermal diffusion to the top of the PT.

The major difficulty with the alternative hypothesis is that the postulated bare surface of the PT material at the groove in the EF, would have been distributed over 360° by the RJ rolling process,

such that the electrochemical diffusion would have occurred axisymmetrically, not just at the top of the PT.

Therefore, in order for the alternative local electrochemical theory to replace the thermal diffusion theory, a reason must be found for the postulated damage of the PT oxide layer being limited to the top of the PT.

It is possible that a small detail of the rolling process could provide a reason for the damage to be concentrated at the top of the PT.

7. Conclusions

1. Based on the assessment of Section 5.1.1, the measured circumferential [H] and [D] gradients in the outlet PT RJ of B6S13 could not have been caused by thermal diffusion alone, under the expected operating temperature profile, depicted in Figure 19 (derived from Figure 10).
2. Provided that Figure 19 accurately represents the operating temperature profile of the B6S13 outlet, it follows that another diffusion mechanism, instead of thermal diffusion to the top of the PT, was responsible for elevated H and D concentrations at the top of the outlet PT in B6S13 and B3F16.
3. Conclusions 1 and 2 are dependent upon the currency and applicability of Figure 19 to B6S13. Given that Bruce Power has asserted that the thermal diffusion theory has been independently verified but no details of the verification process were provided in the documents that were reviewed, no definitive conclusion about the thermal diffusion theory will be drawn at this time.
4. From the assessment of Section 5.2, a potential cause for the circumferential H and D concentration gradients observed in the outlet PT RJ of B6S13 could be electrochemical diffusion from the EF grooves into the PT, although there is no current explanation for why the ingress source would be limited to the top of the PT.

8. Recommendations

1. It is recommended that Bruce Power issue the details of the operating thermal gradients in B6S13 that were cited as the cause of thermal diffusion of H and D to the top of the PT.

9. References

1. Predicting Deuterium Concentrations in Pressure Tubes at Rolled Joints, COG-94-509, A.A Bahurmuz, M, B. Elmosheli, V.F. Urbanic, September, 1994.
2. DIFFUSION COEFFICIENT MODELLING IN Zr 2.5%Nb FOR USE IN PROBABILISTIC ROLLED JOINT DEUTERIUM UPTAKE ASSESSMENTS OF CANDU REACTORS, Transactions, SMiRT-25 Charlotte, NC, USA, August 4-9, 2019 Division I, E. Nadeau, D. Metzger, Candu Energy Inc.
3. Molecular Dynamics Study of Hydrogen in α -Zirconium, Ravi Kiran Siripurapu,¹ Barbara Szpunar,² and Jerzy A. Szpunar¹, ¹Department of Mechanical Engineering, University of Saskatchewan, 57 Campus Drive, Saskatoon, SK, Canada S7N 5A9, ²Department of Physics and Engineering Physics, University of Saskatchewan, 116 Science Place, Saskatoon, SK, Canada S7N5E2, Published 9 November, 2014.
4. Fluid flow in a diametrically expanded CANDU fuel channel – Part 2: Computational study, M.H.A. Piro , M. Christon, B. Tensuda , M. Poschmann, M. Bruschewski, S. Grundmann, C. Tropea Elsevier Nuclear Engineering and Design, September, 2019.
5. Hydrogen Permeability through n-type Cr₂O₃ Scale at 1273 K under the Oxygen Activities of 1.6×10^{-18} – 1.0×10^{-16} , Minoru TANAKA, Mitsutoshi UEDA, Kenichi KAWAMURA and Toshio MARUYAMA, ISIJ International, Vol. 51 (2011), No. 4, pp. 638–644.
6. Hiroji KATSUTA & Kazuo FURUKAWA (1981) Hydrogen and Deuterium Transport through Type 304 Stainless Steel at Elevated Temperatures, Journal of Nuclear Science and Technology, 18:2, 143-151, DOI: 10.1080/18811248.1981.9733235
7. Hydrogen in Zirconium. Part I, T.P. Chernyayeva, A.V. Ostapov, Voprosy atomnoj nauki i tehniki = Pytannja atomnoj nauky i techniky = Problems of atomic science and technology 87(5), July 2013.

10. Appendix 1- Summary of Diffusion Calculations to Test the Alternative Theory

A1.1 Estimation of the Rate of Mass Flow of D from the Local Volume at the Top of the B6S13 Outlet PT RJ by Fick's Diffusion

Section A1.1 presents Tables A1-1 through A1-4b, which detail the D diffusion calculations performed to estimate the D mass flow rate from the top of the PT, referred to in Section 5.2.3 as a test of the alternative theory.

Table A1-1 provides a summary of the [D] gradient calculation for axial diffusion out of the local volume, using Equation 4b. A definition of the variables is presented below the table.

Table A1-1

Linear Axial [D] Gradient Calculation									
x_1	x_2	Δx	C_{1x}	C_{2x}	ΔC	$\partial c/\partial x$	ρ_{PT}	ΔC	$\partial c/\partial x$
(mm)	(mm)	(mm)	(ppm)	(ppm)	(ppm)	(ppm/m)	(kg m ⁻³)	(kg m ⁻³)	(kg m ⁻⁴)
28	44	0.016	520	450	70	4375	6440	0.451	28.175

x_1	Axial start of the local volume, measured from the end of the PT
x_2	Axial end of the local volume, measured from the end of the PT
Δx	Axial length of the local volume
C_{1x}	D concentration at x_2
ρ_{PT}	Density of the PT material
C_{2x}	D concentration at a point inboard x_2
ΔC	Difference in D concentration
$\partial c/\partial x$	Axial D Concentration gradient

Similarly, Table A1-2 details the [D] gradient calculation for axial diffusion out of the local volume, again for use in Equation 4b.

Table A1-2

Calculation of Circumferential Gradient for Curve Fit to [D] vs θ									
θ_1	θ_2	$\Delta\theta$	r_m	Δy	$\partial c/\partial\theta$	ΔC	ρ_{PT}	ΔC	$\partial c/\partial y$
(rad)	(rad)	(rad)	(m)	(m)	(ppm/rad)	(ppm)	(kg m ⁻³)	(kg m ⁻³)	(kg m ⁻⁴)
0	0.8	0.8	0.0540	0.043	235.9	188.7	6440	0.122	2.811

θ_1	Angular position at the top of the local volume
θ_2	Angular position at the edge of the local volume
$\Delta\theta$	Difference in angular position
r_m	Mean radius of the PT
Δy	Change in position in the y direction corresponding to $r_m \Delta\theta$
$\partial c/\partial\theta$	Circumferential concentration gradient
ΔC	Difference in concentration
ρ_{PT}	Density of the PT material
$\partial c/\partial y$	Concentration gradient in the y direction

The calculation of D flux out of the local volume in the axial (x) and circumferential (y) directions are summarised in Table A1-3, with the summary of the resultant predicted D mass flow rate out of the volume given in Table A1-4a.

Table A1-3

Calculation of Axial and Circumferential D Fluxes								
T	T	1000/T	ln D	D	dC/dy	dC/dx	J_{circ}	J_{ax}
(°C)	(K)	(1/K)		(m ² s ⁻¹)	(kg m ⁻³)	(kg m ⁻³)	(kg m ⁻² s ⁻¹)	(kg m ⁻² s ⁻¹)
308	581.15	1.7207	-22.91	1.1E-10	2.811	28.175	-3.164E-10	-3.171E-09

T	Temperature
D	Diffusion Coefficient
dC/dy	D Concentration gradient in the y direction
dC/dx	D Concentration gradient in the x direction
J_{circ}	Circumferential D flux
J_{ax}	Axial D flux

Table A1-4b, provides, in support of Table A1-4a, the dimensions assumed for the local volume at the top of the PT RJ. These dimensions were used to calculate the cross-sectional areas used to predict the mass flow rates of Table A1-4a.

Table A1-4a

Calculation of D Mass Flow out of the Local Volume						
J_{circ}	A_{circ}	\dot{m}_{circ}	J_{ax}	A_{ax}	\dot{m}_{ax}	\dot{m}_{total}
($\text{kg m}^{-2} \text{s}^{-1}$)	(m^2)	(kg s^{-1})	($\text{kg m}^{-2} \text{s}^{-1}$)	(m^2)	(kg s^{-1})	(kg s^{-1})
-3.164E-10	1.17E-04	-7.4E-14	-3.17E-09	3.61E-04	-1.1E-12	-1.2E-12

J_{circ}	Circumferential Flux of D
A_{circ}	Cross-Sectional PT area perpendicular to the circumferential flux
\dot{m}_{circ}	Circumferential mass flow rate of D
J_{ax}	Axial Flux of D
A_{ax}	Cross-Sectional PT area perpendicular to the axial flux
\dot{m}_{ax}	Axial mass flow rate of D
\dot{m}_{total}	Total mass flow rate of D

Table A1-4b

Dimensions of the Local Volume			
L	$w_{\text{PT RJ}}$	r_m	Θ
(m)	(m)	(m)	(rad)
0.028	0.003624	0.0540	1.6

L	Axial length of the local volume
$w_{\text{PT RJ}}$	PT RJ wall thickness
r_m	Mean radius of the PT
Θ	Angular extent of the local volume

Note that in Table A1-4b the PT RJ wall thickness is 3.624 mm versus 4.19 mm for the PT. The reduced wall thickness at the PT RJ is based on a 13.5% wall thickness reduction from the rolling process.

A1.2 Estimation of the Rate of Mass Flow of D for Postulated Electrochemical Diffusion Through Bare Areas of the PT

The calculation, detailed in Table A1-5, was performed using Raoult's law for Electrochemical diffusion which involves the following

parameters: D, the diffusion coefficient
C, the concentration of D in solution
R is the universal gas constant
T is the absolute temperature
 μ is the electrochemical potential of D in solution

It was assumed that the D concentration in the EF was at the solubility limit for D at 308 °C, which was determined from Figure A1-1, divided by the factor 1.1, as per Reference [6], which gave [D] = 3.6 ppm.

Note that the electrochemical potentials for D in Table A1-5 were taken from Refe

Figure A1-1
H Solubility vs Temperature

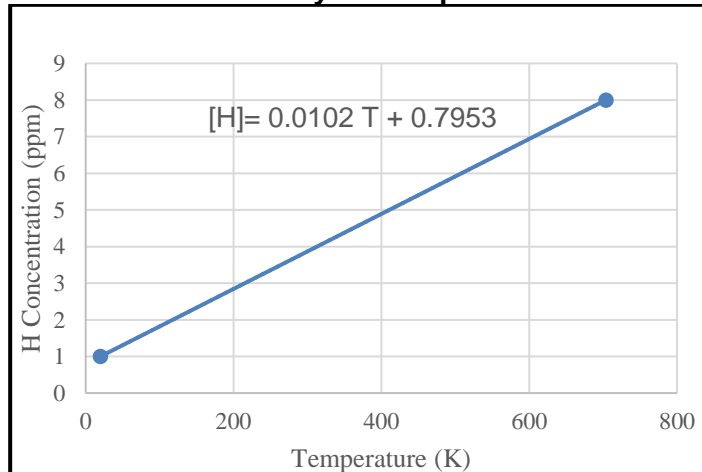


Table A1-5

Calculation of D Flux by Electrochemical through the Postulated Bare Area of the PT										
T	D	C	C	R	Δr	μ in Fe	μ in Zr	$\Delta\mu$	$\Delta\mu/\Delta r$	J
(°C)	(m ² s ⁻¹)	(ppm)	(kg m ⁻³)	(J K ⁻¹ kg ⁻¹)	(m)	(ev)	(ev)	(J kg ⁻¹)	(J kg ⁻¹ m ⁻¹)	(kg m ⁻² s ⁻¹)
308	1.1E-10	3.6	0.023	4129.657	2E-09	-0.2	-0.05	7.2E+06	3.605E+15	0.0039187

T	Temperature
D	Diffusion coefficient
C	D concentration
R	Universal gas constant
Δr	Thickness of the Chromium oxide layer
μ in Fe	Electrochemical potential of D in solution in the EF
μ in Zr	Electrochemical potential of D in solution in the PT
$\Delta\mu$	Electrochemical potential difference
$\Delta\mu/\Delta r$	Electrochemical potential gradient
J	D flux due to electrochemical diffusion

As outlined in Section 5, the diffusion flux in Table A1-5 is exceptionally high, which is attributable, upon deliberation, to the assumption of zero permeability at the interface of the bre PT material with the EF. Table A1-6 provides an estimate of the D flux that can be expected from the EF into the PT material, based on experiments described in Reference [5].

Table A1-6

D Flux through the EF Oxide Layer	
J	J
mol m ² s ⁻¹	kg m ² s ⁻¹
2.00E-05	4.02E-08

For this assessment, the flux in Table A1-6 was assumed as the D flux from the EF to the PT due to electrochemical diffusion.

The elastodiffusion calculations that predict the diffusion of D from the stressed region back into the EF are covered in Tables A1-7a through A1-7c.

Table A1-7a summarises a thermal expansion analysis, used to predict compressive stress on the PT material inside the EF RJ groove.

Table A1-7a

Calculation of Thermal Strain for the PT Material in the Groove								E and σ for PT Groove		
L_{groove}	L_{groove}	CTE_{EF}	CTE_{PT}	DCTE	ΔT	ΔL_{PTG}	ϵ_{PTG}	T	E	σ_H
(in)	(mm)	(m/m)	(m/m)	(m/m)	(°C)	(m)	(m/m)	(°C)	(GPa)	(Gpa)
0.19	4.826	1.3E-06	6.6E-06	5.3E-06	287	7.3E-06	0.00151	308	80.2	0.12107

L_{groove}	Length of the groove in the EF
CTE_{EF}	Coefficient of Thermal Expansion for the End Fitting
CTE_{PT}	Coefficient of Thermal Expansion for the Pressure Tube
DCTE	Differential Coefficient of Thermal Expansion
ΔT	Temperature Increase from 21 C to the operating Temperature of 308 C
ΔL_{PTG}	Differential Axial Thermal Expansion of the PT Material in the EF groove wrt to the EF
ϵ_{PTG}	Axial Thermal Strain in the PT material inside the EF groove from heatup to 308 C
T	Operating Temperature
E	PT Elastic Modulus
σ_H	Hydrostatic thermal stress induced in the PT material in the FF groove

Tables A1-7b and A1-7c cover the elastodiffusion calculations.

Table A1-7b

Summary of Stress Calculation for Elastodiffusion of D back into the EF							
D	S	S	ϕ	V_H	R	T	σ_H^{max}
(m^2s^{-1})	(ppm)	($kg\ m^{-3}$)		($m^3\ mol^{-1}$)	($J\ K^{-1}mol^{-1}$)	(K)	(Pa)
7E-07	3.6	0.023	1	2.00E-06	8.313	581	4E+07

D	Diffusion coefficient D in the EF
S	D concentration in solution in the EF
ϕ	Ratio of S to D solubility
V_H	Molar volume of D on the EF
R	Universal Gas Constant
T	Temperature
σ_H^{max}	Peak hydrostatic stress

Note that in Table A1-7c, $\sigma_H(l)$ was calculated by dividing the peak hydrostatic stress by 45.8, assuming the compressive stress field would propagate into the EF at a 45 degree angle and reach the full EF wall thickness 25.9 mm away from the PT-EF contact face. 45.8 is the ratio of the height of the stress field at the contact face to the thickness of the EF and the peak and remote compressive stresses are assumed to be in the same the same ratio. Δw_{PT} was assigned a value of 0.566 mm on the basis of a PT RJ wall thickness reduction of 13.5%. $d\sigma_H/dx$ in Table A1-7c was approximated as the difference between σ_H^{max} and $\sigma_H(l)$ divided by $w(l)$.

It is seen that the predicted D elastodiffusion flux is insignificant in comparison with the postulated electrochemical flux and the predicted Fick's flux for D.

Table A1-7c

$\sigma(l)$ Calculation of D Flux due to Elastodiffusion back into the EF					
w(l)	ΔW_{PT}	w(l)/ ΔW_{PT}	$\sigma_H(l)$	d σ_H/dx	J
(mm)	(mm)		(Pa)	(Pa/m)	(kg m ⁻² s ⁻¹)
25.908	0.566	45.802	8.81E+05	6.35E+06	4.03E-11

l	Axial distance from the PT material-EF contact face to the position where the compressive stress field has propagated to cover the EF thickness
w(l)	EF thickness
ΔW_{PT}	Height of PT material extruded into the EF groove
w(l)/ ΔW_{PT}	Ratio of material height to EF thickness
$\sigma(l)$	Hydrostatic stress at l
d σ/dx	Hydrostatic stress gradient
J	D flux

As mentioned in Section 5, Table A1-8 presents the D mass flow rate predictions for ingress into the PT from the postulated electrochemical source. It should be noted that the total mass flow into the local volume was taken as the sum of the mass flow from electrochemical diffusion with Cr₂O₃ layer, minus the predicted mass flow from elastodiffusion. To give a total mass flow of 9.471E-12 (kg s⁻¹). Also included in the table is the predicted D mass flow rate by Fick's diffusion from Table A1-4a.

Table A1-8

Summary of D Mass Flow Rate Calculations					
Diffusion Source	Location	Direction	J	A	\dot{m}
			(kg m ⁻² s ⁻¹)	(m ²)	(kg s ⁻¹)
Electrochemical	PT/EF Contact	Into PT	-3.919E-03	0.000226	9.242E-07
Electrochemical with Cr ₂ O ₃ layer	PT/EF Contact	Into PT	4.020E-08	0.000226	9.481E-12
Elastodiffusion	PT/EF Contact	Into EF	4.026E-11	0.000226	9.495E-15
Electrochemical with Cr ₂ O ₃ layer + Elastodiffusion	PT/EF Contact	Into PT	4.016E-08	0.000226	9.471E-12
Fick's Diffusion	Local Volume	Into PT Body			1.217E-12